PLOS ONE

RESEARCH ARTICLE

Determinants of bone damage: An ex-vivo study on porcine vertebrae

Mohammad J. Mirzaali[1☯¤], Flavia Libonati[1☯], Davide Ferrario[1], Luca Rinaudo[2], Carmelo Messina[3], Fabio M. Ulivieri[4]*, Bruno M. Cesana[5], Matteo Strano[1], Laura Vergani[1]

1 Department of Mechanical Engineering, Politecnico di Milano, Milan, Italy, **2** TECHNOLOGIC S.r.l. Hologic Italia, Torino, Italy, **3** Istituto Ortopedico Galeazzi IRCCS, Radiodiagnostic Unit, Milan, Italy, **4** Fondazione IRCCS Cà Granda Ospedale Maggiore Policlinico, Nuclear Medicine-Bone Metabolic Unit, Milan, Italy, **5** Department of Clinical Sciences and Community Health, Unit of Medical Statistics, Biometry and Bioinformatics "Giulio A. Maccacaro", Faculty of Medicine and Surgery, University of Milan, Milan, Italy

☯ These authors contributed equally to this work.
¤ Current address: Department of Biomechanical Engineering, Faculty of Mechanical, Maritime, and Materials Engineering, Delft University of Technology (TU Delft), Delft, The Netherlands
* ulivieri@gmail.com

Citation: Mirzaali MJ, Libonati F, Ferrario D, Rinaudo L, Messina C, Ulivieri FM, et al. (2018) Determinants of bone damage: An ex-vivo study on porcine vertebrae. PLoS ONE 13(8): e0202210. https://doi.org/10.1371/journal.pone.0202210

Editor: Deepak Vashishth, Rensselaer Polytechnic Institute, UNITED STATES

Received: February 9, 2018

Accepted: July 29, 2018

Published: August 16, 2018

Data Availability Statement: All relevant data are publicly available on Harvard Dataverse at the following link: https://doi.org/10.7910/DVN/VNGAGR.

Funding: The authors received no specific funding for this work. TECHNOLOGIC S.r.l. provided support in the form of salary for author LR, but did not have any additional role in the study design, data collection and analysis, decision to publish or preparation of the manuscript. The specific roles of the author are articulated in the author contribution section.

Abstract

Bone's resistance to fracture depends on several factors, such as bone mass, microarchitecture, and tissue material properties. The clinical assessment of bone strength is generally performed by Dual-X Ray Photon Absorptiometry (DXA), measuring bone mineral density (BMD) and trabecular bone score (TBS). Although it is considered the major predictor of bone strength, BMD only accounts for about 70% of fragility fractures, while the remaining 30% could be described by bone "quality" impairment parameters, mainly related to tissue microarchitecture. The assessment of bone microarchitecture generally requires more invasive techniques, which are not applicable in routine clinical practice, or X-Ray based imaging techniques, requiring a longer post-processing. Another important aspect is the presence of local damage in the bony tissue that may also affect the prediction of bone strength and fracture risk. To provide a more comprehensive analysis of bone quality and quantity, and to assess the effect of damage, here we adopt a framework that includes clinical, morphological, and mechanical analyses, carried out by means of DXA, μCT and mechanical compressive testing, respectively. This study has been carried out on trabecular bones, taken from porcine trabecular vertebrae, for the similarity with human lumbar spine. This study confirms that no single method can provide a complete characterization of bone tissue, and the combination of complementary characterization techniques is required for an accurate and exhaustive description of bone status. BMD and TBS have shown to be complementary parameters to assess bone strength, the former assessing the bone quantity and resistance to damage, and the latter the bone quality and the presence of damage accumulation without being able to predict the risk of fracture.

Competing interests: We have the following interests. Luca Rinaudo is employed by TECHNOLOGIC S.r.l. There are no patents, products in development or marketed products to declare. This does not alter our adherence to all the PLOS ONE policies on sharing data and materials, as detailed online in the guide for authors.

Abbreviations: A_0 [mm^2], Primary Area; BMD, Bone Mineral Density; BS [mm^2], Bone Surface; BS/TV [1/mm], Bone Surface to Total Volume; BV/TV [–], Bone Volume to Total Volume; D [–], Damage; DA [–], Degree of Anisotropy; DXA, Dual X-Ray Photon Absorptiometry; E_0 [MPa], Initial Elastic Stiffness; E [MPa], Unloading Elastic Stiffness; F [N], Force; M [–], Fabric Tensor; m_i [–], Eigenvalues; m_i [–], Eigenvectors; MIL [–], Mean Intercept Length; S [mm], Stroke; TBS, Trabecular Bone Score; Tb. N [–], Trabecular Number; Tb.Sp. [mm], Trabecular Spacing; Tb.Th [mm], Trabecular Thickness; ε [%], Strain; ε_y [%], Yield Strain; ε_{ult} [%], Ultimate Strain; μCT, Micro- computed Tomography; ρ_p, Porosity; ρ_s [–], Bone Relative Density; σ [MPa], Normal Stress; σ_y [MPa], Yield stress; σ_{ult} [MPa], Ultimate stress.

1. Introduction

Osteoporosis is a metabolic bone disease characterized by low bone mass and micro-architectural deterioration of bone tissue, leading to enhanced bone fragility and a consequent increase in fracture risk [1]. Osteoporosis also presents a compromised bone strength, as this mechanical property reflects the integration of bone quantity (measured as bone mineral density, BMD) and bone quality (an index related to bone microarchitecture, bone geometry and bone turnover) [1].

BMD is the major predictor of bone resistance to load and fracture, and Dual-X Ray Photon Absorptiometry (DXA) is the gold standard method to measure bone "quantity" [2–4]. Despite its primary role in assessing bone strength, BMD only accounts for about 70% of fragility fractures, while the remaining 30% could be explained by the impairment of bone "quality" parameters that are the geometric and material factors contributing to fracture resistance independently of bone mineral density [3,5,6]. BMD is, indeed, limited by its two-dimensional nature, being areal measurement, and it can not capture the three-dimensional microarchitecture, considered as a key determinant of bone strength [5,7]. Moreover, it is affected by the size and position of the subject [8] and cannot distinguish between the cortical and trabecular compartments. Novel and useful information on the bone microarchitecture can be obtained from the trabecular bone score (TBS) [9–14], a relatively new morphological parameter that can be quickly calculated from DXA (i.e., from 2D-lumbar spine DXA images). In fact, TBS represents a textural measurement, which can provide skeletal qualitative information not obtained by BMD. TBS is based on the experimental variograms of projected gray-level DXA images as reported in [15].

To directly assess the tissue microarchitecture *in vivo* and get high-resolution structural bone parameters, the only available method is the High-resolution peripheral quantitative computed tomography (HR-pQCT) [16–18]. However, it is expensive, not generally available in hospitals, and only applicable to limited sites. The biopsy could be an alternative method for direct assessment of bone microarchitecture [19,20]. It is an invasive procedure though, and does not necessarily reflect the microstructure at sites where the fragility fractures occur, like spine and femur.

The most important parameters, which could be used to improve the clinical assessment of bone fragility, are morphological parameters, such as relative bone density (ρ_s), also measured as Bone Volume to Total Volume (BV/TV), trabecular thickness (Tb.Th), trabecular spacing (Tb.Sp), trabecular number (Tb.N.) [21–23], and the degree of anisotropy (DA) [24–27]. These parameters can be calculated by means of high-resolution imaging techniques such as micro-computed tomography (μCT). μCT-scanning allows one to get the three-dimensional image of the trabecular bone microstructure, whereas ad hoc post-processing techniques allow one to estimate the orientation and distribution of the trabeculae [28].

The relationship between TBS texture parameters and 3D-microarchitecture parameters has been exhaustively studied in the literature [14]. Several ex vivo studies have reported significant correlations between TBS and various bone microstructural parameters assessed by μCT [14,29–31]. In particular, it has been demonstrated that high TBS values correlate with better skeletal texture, as a reflection of higher connectivity density (the manner of how bone trabeculae are overconnected in 3D volume) [32], whereas low TBS values correlate with weaker skeletal texture, as a reflection of degraded micro-architecture [13], and with an increase in prevalent and incident fractures [10]. Besides, recent studies have proved that TBS can discriminate and predict fragility fractures, together with BMD, both in primary and in secondary osteoporosis [33,34].

The effective validity of all the measured morphological and clinical parameters depends on their accuracy as predictors of the mechanical properties of bone, such as compressive strength and elastic stiffness. Several studies have been carried out to find the correlations between DXA, morphological parameters, and the mechanical characteristics. In particular, it has been shown that there is a correlation between BMD and mechanical parameters such as elastic stiffness, strength, and maximum energy absorption [7]. Elastic stiffness has shown to be correlated to TBS [35], and a significant correlation between morphometric and mechanical parameters has also been stated [36,37].

Although most of the studies have been focused on the investigation of the relationship between clinical-morphological parameters and the mechanical ones [38–40], a systematic investigation on the effect of mechanical damage is needed. Vertebral fractures in non-traumatic events are the consequences of damage accumulation and permanent deformation in the vertebral body [41,42]. The accumulation of damage forms microcracks [43–45], which are not detectable by clinical radiographs [46,47]. However, they result in degradation of stiffness and strength and permanent residual strains [41,48–50]. Accumulation of damage in trabecular bone is dependent on site, density, and species [38,48,51–54], and loading mode [55–57]. To validate the use of morphological and clinical parameters as predictors of the effective mechanical properties of bone and fracture risk, also taking into account the potential presence of local damage, a methodical multidisciplinary study, involving the expertise of engineers and medical doctors, is needed.

Considering the current state of the art, the proposed study aims to get an insight into the degradation of bone from a mechanistic point of view, with the goals of determining the sensitivity of the clinical and morphological parameters to the damage accumulation, and their ability in measuring the damage and the risk of fracture. To reach these goals, providing a more comprehensive analysis of bone quality, quantity and damage, we propose a framework that includes clinical, morphological, and mechanical analyses, carried out by means of DXA, μCT and mechanical compressive testing, respectively. DXA allowed us to measure the bone quality in terms of mineral content, mechanical compressive testing allowed us to have a quantitative indication of strength and damage, whereas μCT provided important information about the microarchitecture and its mechanically-induced degradation. This study has been carried out on porcine trabecular bones, as the alignment of the trabeculae, their structural homogeneity and the distribution of the mechanical strength are similar to those of human lumbar spine [37,58].

2. Material and methods

We adopted a combination of different characterization techniques. Fig 1 summarizes the framework followed, composed of the following steps:

a. Collection of lumbar vertebrae from 6 lumbar spines;

b. DXA analysis of lumbar spines;

c. Sample preparation;

d. Analysis of undamaged samples obtained from lumbar vertebrae through:

   c1) DXA;

   c2) μCT;

e. Damage testing of specimens;

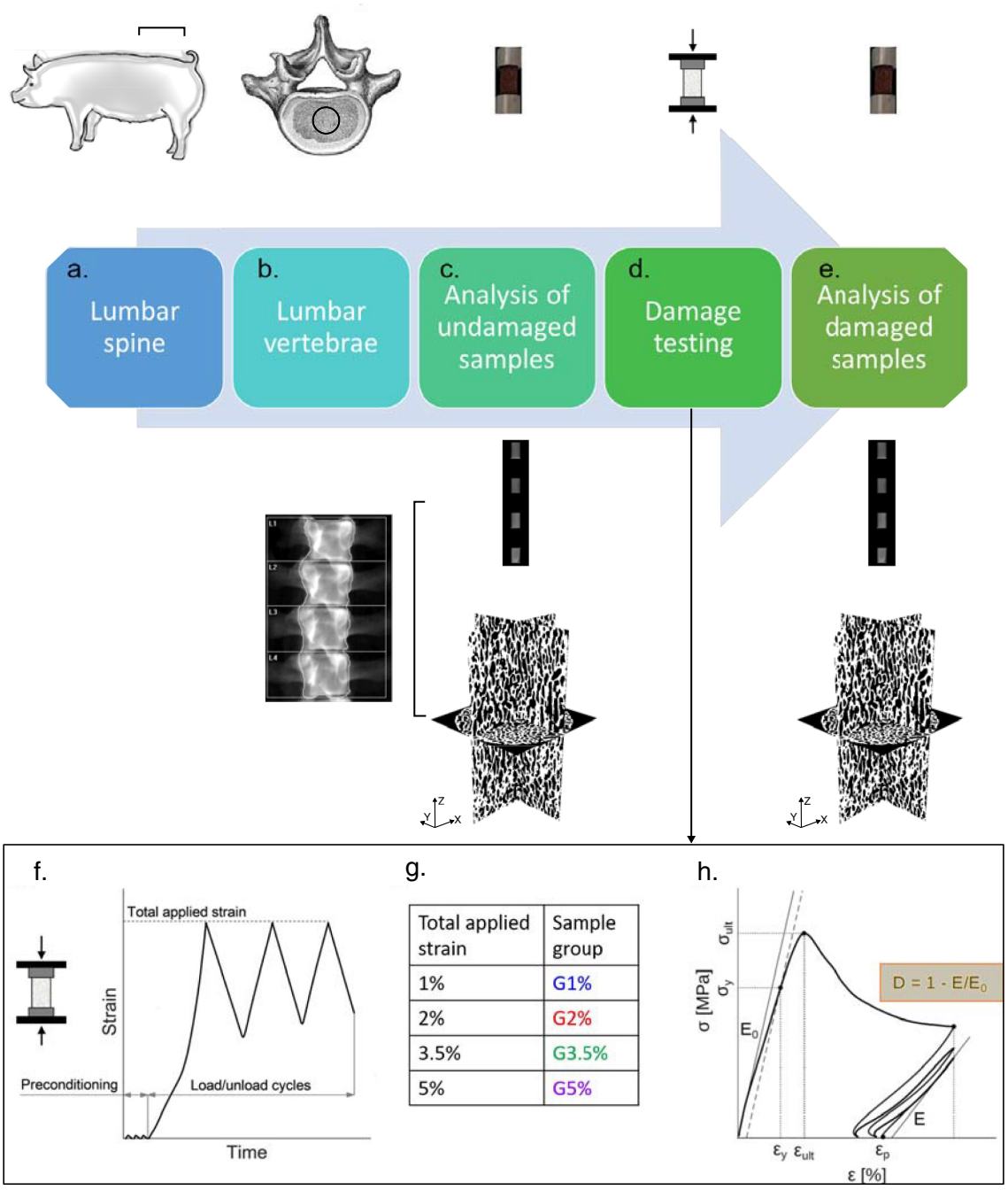

Fig 1. Schematic of the experimental framework adopted. a) Six lumbar vertebrae were taken from pigs and kept frozen. b) DXA was performed on each lumbar body. c) Cylindrical porcine specimens were cut from the core of each lumbar vertebra. DXA scanning was performed for four samples, simultaneously, to get clinical parameters. Then, μCT scanning was performed on each sample to get 3D morphological parameters. d) Porcine specimens were divided into four groups, corresponding to different damage levels, and mechanical compressive tests were performed in each cluster. e) DXA and μCT-scanning were performed on damaged specimens, and corresponding clinical and morphological post-damage parameters were calculated. f) Compressive testing setup and load application: initial preconditioning, followed by three load/unload cycles until a prefixed strain level. g) Nomenclature of the four groups and corresponding total applied strain. h) Schematic of the resulting stress-strain curve and the mechanical properties determined. Damage was calculated as stiffness degradation, as indicated in the yellow box.

https://doi.org/10.1371/journal.pone.0202210.g001

f. Analysis of damaged specimens through:

e1) DXA;

e2) μCT.

Each step is explained in detail in the following.

2.1. DXA Scanning of lumbar spines

Porcine lumbar spines were evaluated with a Hologic Discovery A system (Hologic Inc, Marlborough, Massachusetts, USA) installed at the Bone Metabolic Unit of the Nuclear Medicine of the Fondazione IRCCS Ca' Granda-Ospedale Maggiore Policlinico, Milan, Italy. To assess BMD, we used APEX software installed on the same machine, whereas TBS has been calculated automatically by software provided by Medimaps Group, Wilmington, US, and installed on the same machine. DXA image resolution was set to 0.5 mm, and each spine was placed in accordance to the correct anatomical planes. For each spine, after manually removing the residual ribs left from the butcher, we performed a lumbar scan, manually selecting the region of interest, to calculate TBS for each vertebra. We performed the DXA scanning of each full spine, after removal from the animal, before the sample preparation, to make sure that the clinical parameters of the porcine spines were similar to those of adult human vertebrae, according to the International Society of Clinical Densitometry (https://www.iscd.org/ (April 2016)) and to the National Health and Nutrition Examination Survey (NHANES) [59]. Being the segmentation method in DXA scanning a manual procedure, we tested each vertebra three times to calculate the segmentation effect on our results.

2.2. Sample preparation

Porcine trabecular specimens were cut from six different vertebral columns. The spines involved six lumbar vertebrae from L1 to L6, except for three, where the L6 was missing. At least one specimen was obtained from each lumbar vertebra, leading to a total of 40 samples tested. However, for the following statistical analyses, the duplicates were removed, because two samples extracted from the same vertebra cannot be considered independent from each other. This led to a total of 33 samples. The animals were one year old and porcine lumbar spine vertebrae were provided from a local butcher ("Salumificio Venegoni S.p.A." a store located in Boffalora Sopra Ticino (MI). The vertebral columns were intended for retail trade by the butcher) and then stored at -18˚C till the preparation of the samples and the experimental tests. Samples were drilled using a core drilling device (inner diameter of 16 mm and 40 mm of length) along the anatomical direction of the vertebral column. Subsequently, the samples were transferred to a lathing machine to reduce them to cylinders with the diameter of 13.8 mm and height of 30 mm. During the drilling and turning, the specimens were kept wet by adding water. Then, to reduce the edge effects [60] and eliminate the local damage effect, the ends of the bone samples were glued (3P Scotch-WeldTM EPXTM Adhesive DP490) in custom-made aluminum end caps. The end caps had an inside diameter of 14 mm, outside diameter of 20 mm and height of 15 mm and they covered 3 mm of the specimens on the parallel sides [61]. To obtain perfectly parallel surfaces, both ends of bone specimens were smoothed using a circular blade saw. The bone samples and the aluminum tubes were defatted using acetone before gluing. A custom-made alignment tool was used to keep the bone and the end caps aligned within the direction of axial loading. Specimens were kept frozen at -18˚C, and then rehydrated in saline solution (NaCl 0.9%) at 4˚C for 12 h before mechanical testing.

2.3. Sample imaging

We performed the same scans and analyses on the cylinder samples before and after mechanical testing. In each test, four cylindrical specimens were placed in the machine to perform the DXA scanning, keeping the orientation of the specimens similar to the complete vertebrae. Scanning lasted for about two minutes, and samples were kept frozen before and after scanning, to prevent any deterioration of the microstructure of the bones.

Micro-computed tomography (μCT) images of trabecular specimens were collected using an X-ray Metrology CT system (X25, North Star Imaging Inc., Buckinghamshire, UK) with the spatial resolution of about 25.6 μm. Parameters of the scanning were fixed at 60 kV and 150 μA. Simultaneously, three specimens were placed in the CT equipment and total imaging time was 110 minutes. Specimens were submerged in saline solution during the scanning.

Image reconstruction was performed with the x-view CT software. Image analysis has been performed in ImageJ [62] software and BoneJ plugin [63]. The noise was removed from the images, by using a Gaussian blur filter (standard deviation of the Gaussian distribution 1.5). Thereafter, the images were converted to gray-level 8-bit images. The Otsu local thresholding method [64] was used for the segmentation of the images, resulting in binary images with the voxel value of 1, for bone, and 0, for the empty spaces. Porosity (ρ_p) was defined as the total number of cavities to the total number of voxels in ROI (region of interest) in the binary image. The relative density was defined as $\rho_s = 1 - \rho_p$. Trabecular thickness (Tb.Th) and trabecular spacing (Tb. Sp) were calculated based on the conventional definition of the greatest sphere diameter that fits within the structure [65]. Bone surface (BS) was defined as the inside surfaces of the bone materials and was calculated by the isosurface creation of the binary image with the resampling equal to 1 [66].

The main direction of the microstructures of the bones was measured by Mean Intercept Length (MIL) [27]. It has been shown that an ellipsoid can approximate MIL in three-dimensions [25], and lead to the definition of a positive definite second-order fabric tensor that characterizes the degree of anisotropy of the bone microstructures. Moreover, based on the general theory, developed by [67], the fabric tensor, which is the inverse of MIL tensor, has been applied to measure the local structural anisotropy. Based on the distinct eigenvalues, the fabric can be isotropic, transversely isotropic or orthotropic [68]. The degree of anisotropy (*DA*) can be defined as the complement to the unity of the ratio of the smallest over the largest fabric eigenvalue $DA = 1 - \frac{\min(\mathbf{m_i})}{\max(\mathbf{m_i})}$.

2.4. Mechanical damage tests

Monotonic compression tests were carried out in an MTS machine (Alliance, RF/150) with a load cell of 150 kN (class 1 ISO 7500–1). The specimens were loaded in displacement control along the central cylindrical axis. The axial strain was measured using an extensometer (MTS 632.26F-20 with 8 mm gauge length) attached to the sample. The quasi-static test was performed at a strain rate of 0.0002 s^{-1} (constant stroke rate of 0.05 mm/s). A schematic of the testing protocol adopted is provided in Fig 1F–1H. The loading protocol contained three preconditioning compression cycles up to 0.1% axial strain, followed by monotonic loading until certain strain levels. After that, the specimens were unloaded and loaded three times until the same strain level, to obtain damage and residual plastic strain (Fig 1F). The specimens were divided into four groups, each set loaded until reaching a different strain value. In particular:

- Group 1, called *G1%*, which includes the specimens loaded until 1% of strain, close to the yield strain;

- Group 2, called *G2%*, which includes the specimens loaded until 2% of strain, close to the ultimate strain;
- Group 3, called *G3.5%*, which includes the specimens loaded until 3.5% of strain;
- Group 4, called *G5%*, which includes the specimens loaded until 5% of strain.

All the tests were conducted at room temperature. Data were acquired at a sampling rate of 20 Hz. The recording included time (s), stroke (S), force (F), and axial strain (ε). Normal stress ($\sigma\sigma$) was defined as the ratio of axial force (F) to primary area (A_0), obtained from μCT scans for each sample. The initial elastic modulus (E_0) was calculated using a moving regression with a box width of 0.2% strain to identify the stiffest section of the loading part [55,57]. The yield stress (σ_y) and yield strain (ε_y) were obtained based on a 0.2% offset criterion. The ultimate stress (σ_{ult}) was attained as the maximum primary stress before densification and its corresponding strain as ultimate strain (ε_{ult}). Unloading stiffness (E) was calculated from the steepest part of the last loading cycle. Damage (D) was defined as:

$$D = 1 - \frac{\mathrm{E}}{E_0} \tag{1}$$

2.5. Statistical analysis

An unbalanced Latin Square design was used for mechanical testing. A statistical analysis was carried out in MATLAB® (R2015a) and SAS 9.2, and a p-value < 0.05 was assumed as the significant level. Morphological, clinical and mechanical parameters were analyzed with simple linear regression models to find possible relationships.

ANCOVA was used to test the effect of group, location (fixed factors), and animal (random factor) on the difference of the considered variables between "before" and "after damage", with the "before damage"-value as the covariate. Multiple pairwise comparisons between the group levels have been carried out by means of the Tukey's HSD test with the p-value adjusted for multiplicity. In addition, a test of the null hypothesis that the difference between "before" and "after" damage is equal to zero has been carried out on the estimated least squares means of each group with a significance level of 0.0125, according to the Bonferroni's correction.

3. Results

Fig 2 shows how the clinical (BMD and TBS), morphological (BV/TV, BS/TV, Tb.Sp, Tb.Th, DA), and mechanical (E) parameters are affected by four different mechanical damage levels (G1%, G2%, G3.5%, and G5%). Table 1 summarizes the adjusted linear correlation between mechanical, morphological and clinical parameters.

3.1. DXA scanning

As the DXA segmentation was performed manually, we checked the reproducibility of our results by repeating the scans three times. The coefficient of variation is smaller for entire vertebra than for small specimens. Indeed, results show that for the entire vertebra there is a coefficient of variation of 1.64% and 1.31% respectively for BMD and TBS, by considering the average of the results obtained by three measurements. The coefficient of variation measured from the three repetitions of the measurements for the porcine trabecular specimens for BMD and TBS are 10.04% and 10.73%, respectively.

For the entire porcine vertebra, the mean ± standard deviation of BMD and TBS are 1.16 ± 0.12 g/cm^2 and 1.58 ± 0.08, respectively. The clinical parameters of the individual specimens were significantly different from those of the entire vertebra. Indeed, by reducing the

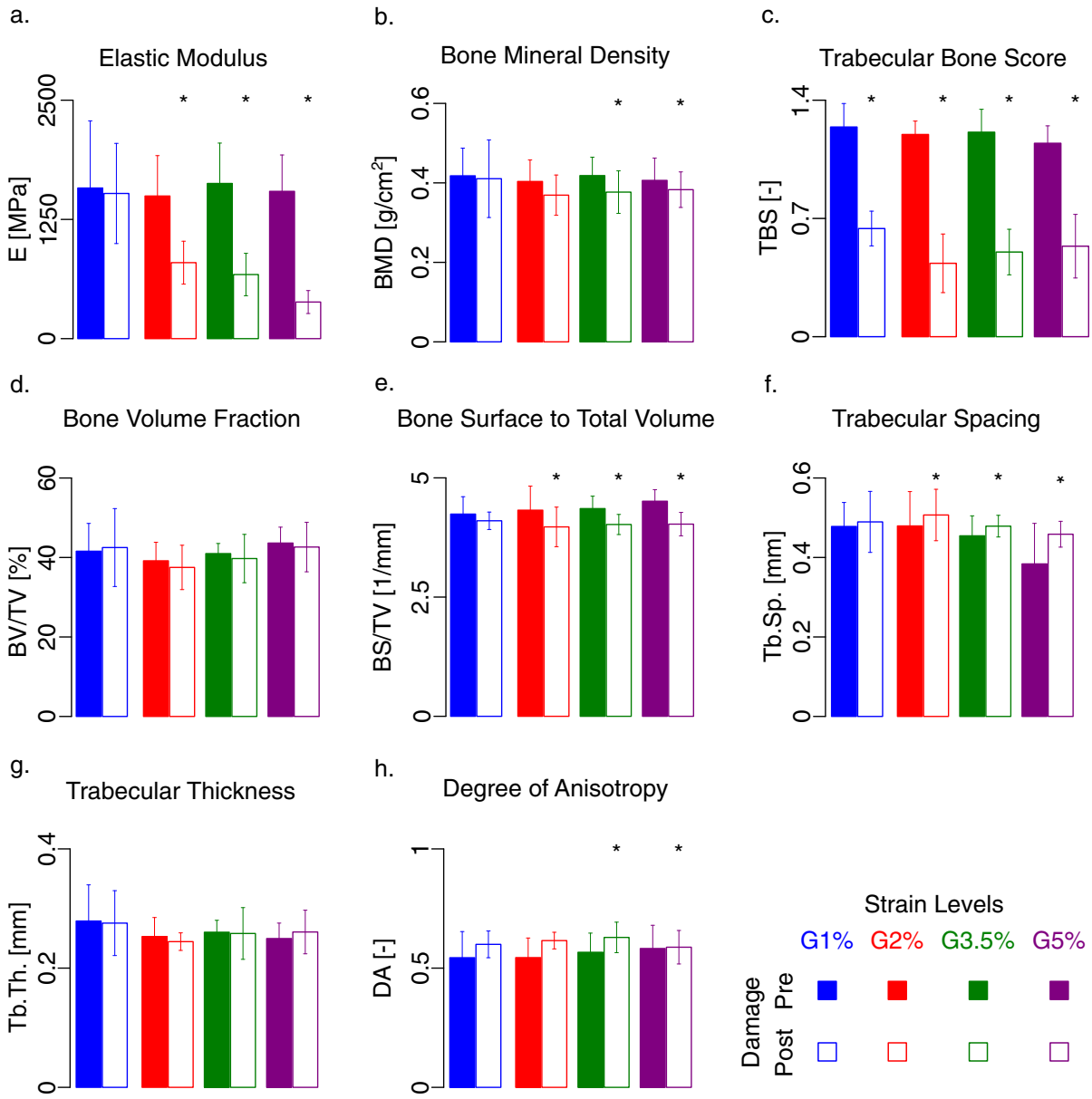

Fig 2. Variation of mechanical (E), clinical (BMD and TBS) and morphological parameters (BV/TV, BS/TV, Tb.Sp, Tb.Th, DA), -before and after damage—for each mechanical damage level (G1%, G2%, G3.5%, and G5%). The filled bars represent the results before damage and the unfilled ones after damage; the labels on the abscissa indicate the damage level. a) Elastic modulus significantly changes within the different group. b) BMD is not affected by the presence of damage. c) TBS significantly changes due to post-yield damage, although no significant difference has been observed between different post-yield damage levels. d) BV/TV does not change through damage loading. The variation of BS/TV (e) and Trabecular spacing (f) is nonzero for the three mechanical groups, G2%, G3.5%, and G5%. g) Trabecular thickness remained the same after applying the damage. h) The degree of anisotropy significantly changes for groups 3.5% and 5%. Asterisk sign shows the significant level ($p < 0.0125$) in the case of comparison, based on the ANCOVA tests.

https://doi.org/10.1371/journal.pone.0202210.g002

size of the vertebra and producing the cylindrical samples, the mean ± standard deviation will change to 0.41 ± 0.05 g/cm^2 for BMD and 1.19 ± 0.11 for TBS, as the cortical part of the vertebra is removed for the trabecular specimens.

Clinical parameters (BMD, TBS), were similar between animals and vertebral locations ($p > 0.05$). Therefore, we were able to pool the results (S1 and S2 Table). We found that BV/

Table 1. Adjusted linear correlations (R^2) between mechanical properties, morphological and clinical parameters. In case of significant linear correlation ($p < 0.05$), the corresponding cells are gray-highlighted. Results are obtained from micro-CT scan before the damage tests.

	BMD	TBS	E_0	ε_y	σ_y	ε_{ult}	σ_{ult}	BV/TV	BS	BS/BV	BS/TV	TbTh	TbSp	SMI	DA
BMD	1.00	0.03	0.20	-0.03	0.23	-0.03	0.34	0.21	0.02	0.26	-0.03	0.23	-0.03	0.17	-0.03
TBS		1.00	-0.03	0.13	0.10	-0.04	-0.03	0.22	0.07	0.09	0.06	0.03	0.01	0.12	-0.02
E_0			1.00	0.18	0.42	0.16	0.67	-0.02	0.01	-0.01	-0.03	-0.03	-0.02	0.06	0.09
ε_y				1.00	0.08	0.01	-0.01	-0.01	0.15	-0.03	-0.01	-0.03	-0.03	-0.02	-0.04
σ_y					1.00	0.08	0.76	0.07	0.26	0.04	-0.02	-0.02	-0.04	0.17	0.07
ε_{ult}						1.00	-0.04	-0.02	-0.04	-0.02	-0.04	-0.03	-0.04	-0.04	-0.05
σ_{ult}							1.00	0.09	0.35	0.04	-0.01	-0.01	-0.04	0.18	0.18
BV/TV								1.00	0.10	0.51	0.30	0.21	0.42	0.48	0.07
BS									1.00	-0.02	0.43	0.05	0.10	0.27	0.07
BS/BV										1.00	-0.01	0.56	0.02	0.23	0.10
BS/TV											1.00	0.03	0.43	0.13	-0.03
TbTh												1.00	-0.03	-0.03	0.21
TbSp													1.00	0.14	-0.01
SMI														1.00	0.01
DA															1.00

https://doi.org/10.1371/journal.pone.0202210.t001

TV is linearly related to BMD ($R^2 = 0.21$) and to TBS ($R^2 = 0.22$). By comparing the clinical and the morphological parameters, we found a linear relationship between BMD and the other morphological parameters, such as BS/BV ($R^2 = 0.26$), and Tb. Th ($R^2 = 0.23$) ($p < 0.01$) (Table 1).

By observing the values of BMD and TBS, we can notice how the clinical parameters significantly changed after mechanical loading ($p < 0.05$). The effect of different damage levels on clinical parameters is depicted in Fig 2B and 2C. In particular, the variation of BMD (Fig 2B) differs from zero for G3.5% and for G5% ($p < 0.01$). The variation of TBS (Fig 2C) is statistically significant for the four mechanical groups ($p < 0.01$). However, we could not define a damage parameter able to quantitatively describe the effect of different damage levels on TBS values.

3.2. μCT-analyses

The tests showed that all morphological parameters do not depend on the location of the spine and the animal ($p > 0.05$). Morphological parameters in this study are in the same range of reported values in the literature [69]. Morphometric properties are reported in S3 Table.

We found a linear relationship between BV/TV and different morphological parameters such as BS/BV ($R^2 = 0.51$), BS/TV ($R^2 = 0.30$), trabecular thickness (Tb.Th) ($R^2 = 0.21$) and trabecular separation (Tb.Sp) ($R^2 = 0.42$) ($p < 0.005$).

The correlation between the bone surface (BS) and relative bone volume (BV/TV) for human trabecular bone has already been reported before [70]. From our results, we also found a direct correlation between BS/TV and Tb.Sp ($R^2 = 0.10$, $p < 0.05$). Similar linear correlation was found between BS/TV and BV/TV ($R^2 = 0.10$, $p < 0.05$), as shown in Table 1.

Fig 2D highlights the variation of BV/TV with respect to the undamaged specimens for each damage level. Statistical analysis confirmed no significant reduction of BV/TV neither for each level of damage nor between the damage levels (Fig 2D). BS/TV (Fig 2E) shows a significant reduction for the groups after yield. Tb.Sp significantly varies for G2%, G3.5% and G5% ($p < 0.005$) (Fig 2F), whereas the variation of DA is significant for G3.5% and for G5%

($p < 0.01$) (Fig 2H). No significant changes were observed for the other morphological parameters such as Tb.Th (Fig 2G).

3.3. Mechanical damage tests

The mechanical properties in the four groups are similar ($p > 0.5$). Therefore, we pooled these data to calculate the mean value of the mechanical properties (see S4 Table).

Mechanical properties determined from the porcine samples are in the same range of the values reported in the literature [71,72].

We tried, then, to find a correlation between the clinical, morphometric and mechanical parameters. Fig 3 shows the trend of the mechanical parameters (E_0 and σ_{ult}) with respect to the clinical ones (BMD and TBS) and to a morphometric parameter (BV/TV). It is found a weak correlation of E_0 with BMD ($R^2 = 0.20$; $p = 0.005$), σ_{ult} and BMD ($R^2 = 0.34$; $p = 0.002$). The correlation with other parameters is provided in Table 1. The yield stress, σ_y, showed a weak correlation with BMD ($R^2 = 0.23$; $p = 0.005$) and TBS ($R^2 = 0.10$, $p = 0.046$) (Table 1). No significant linear trend was found between the mechanical properties (E_0 and σ_{ult}) and the parameters TBS and BV/TV. The bone strength, measured as ultimate stress (σ_{ult}) is linearly related to DA ($R^2 = 0.18$, $p = 0.02$). On the contrary, there is no statistical association between ultimate and yield strain and other morphometric and clinical parameters.

The variation of the elastic modulus (Fig 2A) is the only variable that significantly changes within the different groups ($p < 0.001$, ANCOVA); in particular, G1% is different from G2%,

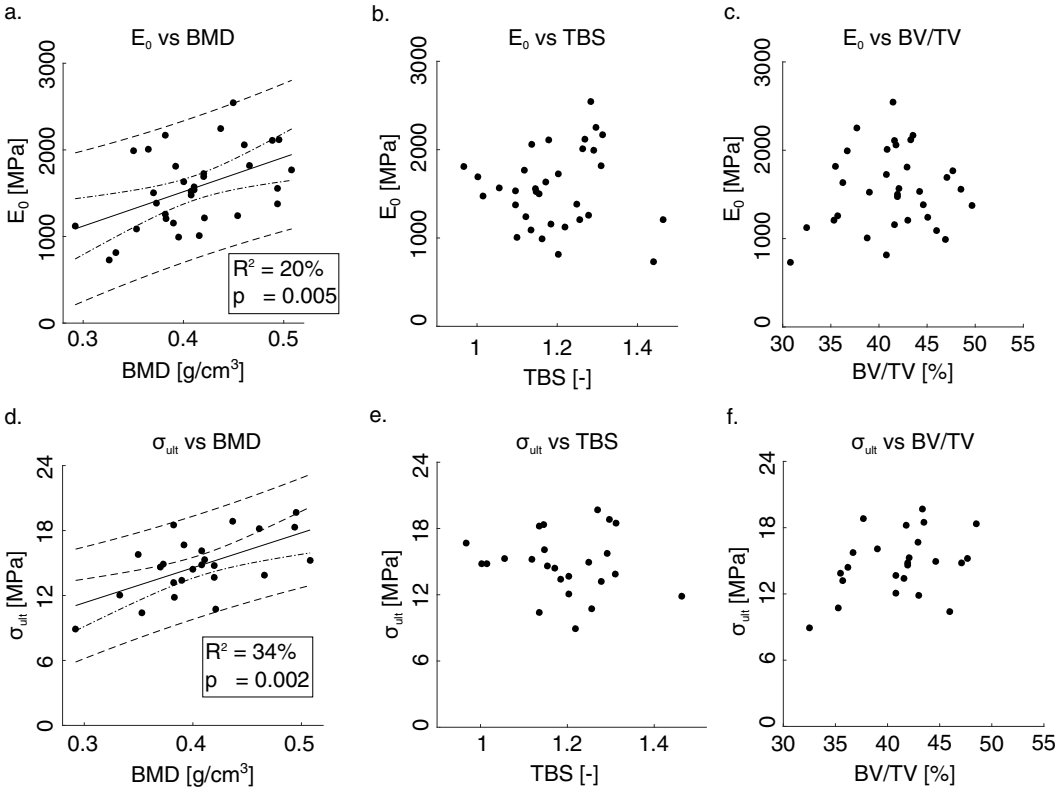

Fig 3. Variation of the elastic stiffness and strength with the BV/TV and other clinical parameters (BMD and TBS). In the case of significant correlation between each parameter, a linear regression line is specified. $R^2 = 0.20$; $p = 0.005$ in a) and $R^2 = 0.34$; $p = 0.002$ in d). The dashed lines are referred to confidence and prediction intervals. Regression lines are added only for significant correlation.

https://doi.org/10.1371/journal.pone.0202210.g003

G3.5%, and G5%, whereas G2%, G3.5%, and G5% show a similar average value. The variation of E is significantly different from zero for G2%, G3.5% and G5% ($p < 0.005$).

4. Discussion

Direct assessment of bone resistance to fracture and damage requires mechanical testing, which is not possible to be included in a clinical protocol. Here, to investigate the effect of damage on bone quality and quantity, we identified four damage levels (as four levels of strain, in both the elastic and the post-yield regions) and we carried out compressive tests on samples of trabecular bone to induce mechanical damage. We analyzed all the parameters that could be involved in the damage process. We used a combination of different characterization techniques to provide a thorough analysis of bone quality and how it is affected by the presence of damage. The effect of damage accumulation in the trabecular bones has been analyzed from different points of view: i) clinical, ii) morphological, and iii) mechanical.

From a **clinical point of view**, BMD has shown to be an indicator of bone quantity more than quality, taking into account the presence of mineral and not the presence of damage. Indeed, from statistical analyses, we found significant changes in BMD only for the specimens subjected to damage larger than 3.5% strain (Fig 2B and Fig 4A). However, we should underline that being the resolution of the DXA scanning images not high enough, it was not possible to detect the microcracks propagated in the specimens during the overloading. BMD resulted in the best predictor of mechanical parameters, despite the weak correlation factors.

TBS has shown to be a quality index that is markedly affected by the presence of damage (Fig 2C and Fig 4B). This is consistent with previous evidence of using TBS as a risk factor and its role as a complementary to the BMD [10,14,73]. Our results indeed, exhibit a significant change in the TBS before and after damage, due to the alteration of the microstructure of the trabecular bone under severe mechanical damage loadings. The decrease of TBS is about 50% when the applied strain is larger than 1%. It seems that if the elastic limit is reached, the TBS values are strongly affected by the damage, more than the other morphological parameters,

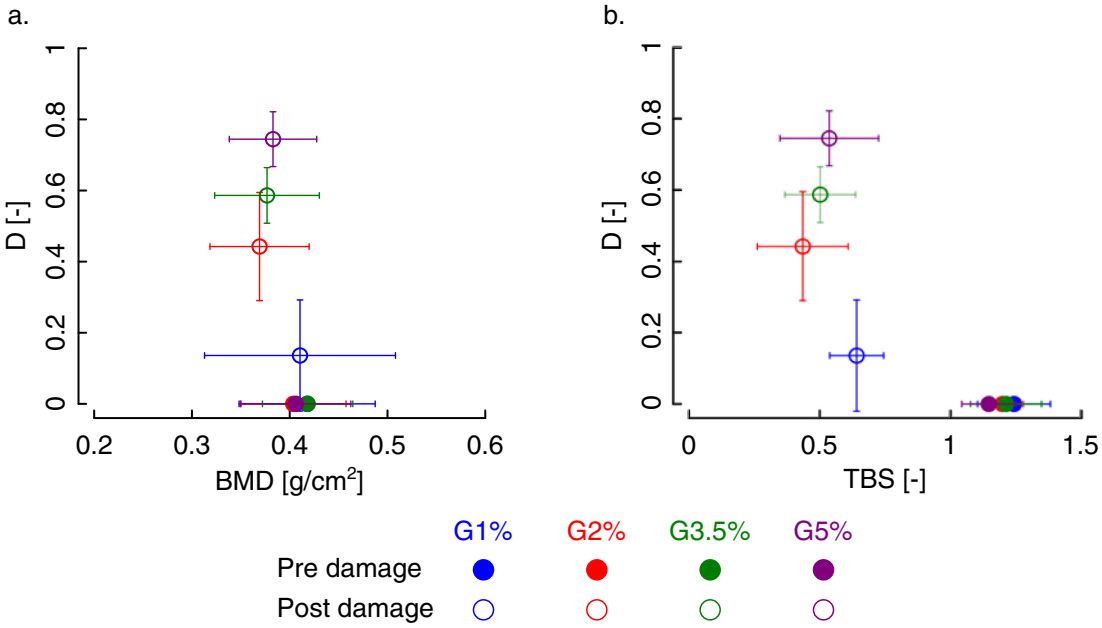

Fig 4. Comparison of accumulated damage obtained from different strain levels with a) BMD and, b)TBS.

https://doi.org/10.1371/journal.pone.0202210.g004

which exhibit significant but smaller variations. However, TBS is not able to distinguish between the different damage levels (Fig 4B). After the first level, corresponding to a loading level close to the yield strain, in fact, the values of TBS are markedly smaller than the values of undamaged specimens but not significantly different from each other. TBS, therefore, seems to be able to identify a damaged bone but not to quantify the damage itself. Furthermore, we did not find any correlation between TBS (before and after damage and their ratios), and damage, meaning TBS ($p>0.05$) can only qualitatively describe damage but not quantitatively (Fig 4B). There is not any relationship between TBS and plastic strain ($p > 0.05$) as well.

We also found a significant linear correlation between TBS and the parameters BV/TV. TBS is a 2D representation of a 3D microstructure. In 3D, microstructural changes can be captured by BV/TV, and in 2D, our results show TBS can effectively do the same. Although for the human trabecular bone, it is shown that BV/TV and fabric tensor are a better determinant of stiffness than TBS [74]. DXA was performed on both lumbar spines and trabecular specimens obtained from the spines. The size of the specimens is the largest size that we could obtain within the dimensions of the porcine vertebra. As the aim of this study was to determine the tissue mechanical properties, and how such properties are affected by mechanical damage, we could not perform the test on the whole vertebra. However, we believe that increasing the size of the specimens makes it easier to select the area for the DXA measurements.

Comparison of TBS and BMD for the entire porcine vertebra with the data for human lumbar spine showed that our results are in the same range of the reported data in the literature [9], thus assessing the validity of this study. However, the bone fraction (BV/TV) shows slightly higher value compared to the human vertebra. This difference could come from the rather young porcine samples in our study.

From a morphological point of view, we found significant changes in several morphological parameters after yielding, indicating how a higher level of damage affects the microarchitecture.

In particular, we can observe a significant change of BS/TV in damage groups after yielding, i.e. G2% to G5%. It has been shown in [75] that local failure initiates in the sub-regions with smaller BV/TV. This makes smaller total volume, as we also observed in our experiments, which could increase BV/TV and decrease BS/TV. Although we did not find a significant increase for BV/TV, the individual observation of TV for each specimen showed a significant decrease specifically for those specimens that were tested after yielding. We also observed that bone volume for the samples tested after yielding diminishes, balancing the total volume reduction. We also did not find any significant correlation between BV/TV and damage.

Trabecular spacing (Tb.Sp.) also showed a significant reduction for the post-yield groups. This could be justified by microscopic damage and propagation of microcracks in the trabeculae under severe damage loading [53,76–78]. As we performed the μCT scans in the wet condition, the fractured trabeculae could be washed away, producing larger interspacing between trabeculae. We did not perform labeling of microcracks in this study. Therefore we could not measure the size of the microcracks in the post-yield mechanical loading. Owing to the size of microcracks in the trabecular bone, synchrotron CT imaging at the resolution of less than 1μm will be adapt to precisely detect the microcracks in bone [77,79–82].

The degree of anisotropy showed a significant change after damage for groups G3.5% and G5%. This parameter is a scalar parameter that does not provide more information about the orientation of the trabeculae. A more in-depth investigation of the results showed that the largest eigenvalue after and before damage remained the same, whilst, the smallest eigenvalue decreased for the specimens after damage. Based on the definition of MIL [27] and fabric tensor [67], the angle between the largest diameter of the ellipsoid and z-axis did not change after

damage, while the angle of two other diameters of the ellipsoid and z-axis changed significantly. This shows that the orientation of the microstructure (trabeculae) changes due to the compressive loading. In other words, the fitted ellipsoid became elongated along its major axis while its minor axis rotated toward the loading direction (z-axis). This can also be inferred from the increase in DA, as it means higher anisotropy in the microstructure of the trabecular bone due to the induced damage.

Trabecular specimens in this study showed a plate-like structure due to visual observation from micro-CT scans. It was reported in the past that damage fraction area is higher in the plate-like rather than rod-like trabecular structures [53,83,84]. Nevertheless, we did not measure such damage fraction area.

From a mechanical point of view, the increase of damage level resulted in a stiffness degradation, which is significant above the yield limit. In the last group, where the strain level reaches 5%, we observed about 80% of stiffness degradation due to the microdamage propagation in the trabecular bone. This is in line with the results of compressive damage tests on trabecular bones previously reported in the literature [57,85,86]. The damaged specimens showed barreling and macroscopic shear plane fracture after yielding, similarly to the reported data for human [75] and bovine trabecular bone[61].

The elastic stiffness ($R^2 = 0.2$, $p = 0.005$) and strength ($R^2 = 0.34$, $p = 0.002$) of trabecular porcine in this study were linearly correlated to the bone mineral density (BMD). The strong correlation between these primary mechanical properties and BMD has been reported for the human trabecular bone of proximal femur which were $R^2 = 0.57$ for elastic stiffness, and $R^2 = 0.82$ for strength [7]. Although we did not find any significant correlation between TBS and primary mechanical properties, i.e., elastic stiffness and strength, a significant linear correlation between TBS and the elastic stiffness for human lumbar vertebrae ($R^2 = 0.41$; $p = 0.007$) has been reported [30]. A significant correlation between bone volume fraction (BV/TV) and elastic stiffness ($R^2 = 0.82$, $p = 0.002$) and strength ($R^2 = 0.87$, $p < 0.001$) were reported for the cubic-shape trabecular bone specimens obtained from porcine vertebrae [37]. Our results do not show such significant correlation between BV/TV and those primary mechanical properties, which can be due to the small variation of BV/TV values of specimens tested in this study. However, the mechanical properties in this study are within the range of ones reported in [37].

One of the limitations of this study is related to the characterization tools that we used for the determination of damage. We quantified damage from the mechanical point of view based on the degradation of stiffness, and we did not characterize it by measuring the damage surfaces/volumes using staining protocols that have been used for micro-CT images [87,88]. Those data could have been used to check the sensitivity of clinical parameters specifically TBS and other morphological parameters in the formation of microcracks.

5. Conclusion

Bone's resistance to fracture depends on several factors: the bone mass, the microarchitecture, including the geometry and distribution of the trabeculae, and the tissue material properties. Here, the adoption of multiple characterization techniques provided a more comprehensive analysis of bone parameters and how they are affected by the presence of damage. The possibility of mechanically induced damage of different entity allowed us to perform a systematic study on the effect of different damage levels on bone tissues, from diverse perspectives (e.g., clinical, morphological, and mechanical).

BMD and TBS have shown to be complementary parameters to assess bone strength, the former assessing the bone quantity, the bone resistance to damage, and its loading sensitivity, and the latter the bone quality and the presence of damage. BMD is slightly affected by the

damage (i.e., BMD is only affected by damage level above 3.5% strain), whereas TBS can always be considered as a good indicator of damage, without being able to quantify it though. Moreover, it cannot perfectly explain the risk of fracture in the bone tissue, or how healthy bone is, as we did not find any linear relationship between TBS and the mechanical strength.

The outcome of our DXA analyses is comparable to those provided in the literature for the human lumbar spine [71], proving the similarity of porcine and human trabecular bone from the lumbar spine, and endorsing a more extensive validity of this research.

This study confirms that no single method can provide a complete characterization of bone tissue, and the combination of complementary techniques is required for an accurate and exhaustive description of bone health. Limitations of the current study regard the difficulty of quantifying the damage effect. In future works, we aim to quantify the damage effect, not only from the mechanical perspective but also from the clinical and morphological viewpoints and to monitor the damage evolution. The latter would be possible by performing mechanical testing into a micro-CT scan device. In an ongoing work, we are trying to investigate the effect of damage induced by fatigue loading, coupling experiments with numerical models, able to mimic bone degradation. We believe that numerical models, built from BMD data could provide a valid and versatile tool, easily implemented in the clinical routine, for the assessment of the bone quality and the prediction of the fracture risk.

Supporting information

S1 Table. Supporting information minimal datasheet supplementary document.
(XLS)

S2 Table. Clinical parameters before and after the mechanical testing.
(PDF)

S3 Table. Morphometric properties of the trabecular porcine specimen before damage testing.
(PDF)

S4 Table. Mechanical properties of trabecular porcine specimens.
(PDF)

Acknowledgments

The authors would like to thank Prof. Michele Carboni for helping with μCT imaging, Lorenzo Giudici for helping in mechanical testing, and Luigi Roberto Baglioni for helping in sample preparation.

Author Contributions

Conceptualization: Mohammad J. Mirzaali, Flavia Libonati, Fabio M. Ulivieri, Laura Vergani.

Data curation: Mohammad J. Mirzaali, Flavia Libonati, Laura Vergani.

Formal analysis: Mohammad J. Mirzaali, Flavia Libonati, Davide Ferrario, Bruno M. Cesana.

Investigation: Mohammad J. Mirzaali, Flavia Libonati, Davide Ferrario, Luca Rinaudo, Carmelo Messina, Fabio M. Ulivieri, Matteo Strano, Laura Vergani.

Methodology: Mohammad J. Mirzaali, Flavia Libonati, Luca Rinaudo, Carmelo Messina, Fabio M. Ulivieri, Laura Vergani.

Software: Luca Rinaudo.

Supervision: Mohammad J. Mirzaali, Flavia Libonati, Fabio M. Ulivieri, Laura Vergani.

Validation: Mohammad J. Mirzaali, Flavia Libonati, Fabio M. Ulivieri, Laura Vergani.

Visualization: Mohammad J. Mirzaali, Flavia Libonati, Fabio M. Ulivieri, Laura Vergani.

Writing – original draft: Mohammad J. Mirzaali, Flavia Libonati, Luca Rinaudo, Fabio M. Ulivieri, Laura Vergani.

Writing – review & editing: Mohammad J. Mirzaali, Flavia Libonati, Fabio M. Ulivieri, Laura Vergani.

References

1. Consensus N. Development panel on osteoporosis: prevention, diagnosis and therapy. J Am Med Assoc. 2001; 285.
2. Cameron JR, Sorenson J. Measurement of bone mineral in vivo: an improved method. Science. American Association for the Advancement of Science; 1963; 142: 230–232.
3. Shepherd JA, Schousboe JT, Broy SB, Engelke K, Leslie WD. Executive summary of the 2015 ISCD position development conference on advanced measures from DXA and QCT: fracture prediction beyond BMD. Journal of Clinical Densitometry. Elsevier; 2015; 18: 274–286. https://doi.org/10.1016/j.jocd.2015.06.013 PMID: 26277847
4. Organization WH, others. Assessment of fracture risk and its application to screening for postmenopausal osteoporosis: report of a WHO study group [meeting held in Rome from 22 to 25 June 1992]. Geneva: World Health Organization; 1994;
5. Ammann P, Rizzoli R. Bone strength and its determinants. Osteoporosis International. Springer; 2003; 14: 13–18.
6. Hunt HB, Donnelly E. Bone Quality Assessment Techniques: Geometric, Compositional, and Mechanical Characterization from Macroscale to Nanoscale. Clinical Reviews in Bone and Mineral Metabolism. 2016; 14: 133–149. https://doi.org/10.1007/s12018-016-9222-4 PMID: 28936129
7. Wachter N., Augat P, Mentzel M, Sarkar M., Krischak G., Kinzl L, et al. Predictive value of bone mineral density and morphology determined by peripheral quantitative computed tomography for cancellous bone strength of the proximal femur. Bone. 2001; 28: 133–139. http://dx.doi.org/10.1016/S8756-3282(00)00455-5 PMID: 11165955
8. Bolotin H. DXA in vivo BMD methodology: an erroneous and misleading research and clinical gauge of bone mineral status, bone fragility, and bone remodelling. Bone. Elsevier; 2007; 41: 138–154. https://doi.org/10.1016/j.bone.2007.02.022 PMID: 17481978
9. Bousson V, Bergot C, Sutter B, Levitz P, Cortet B, others. Trabecular bone score (TBS): available knowledge, clinical relevance, and future prospects. Osteoporosis International. Springer; 2012; 23: 1489–1501. https://doi.org/10.1007/s00198-011-1824-6 PMID: 22083541
10. Harvey NC, Glüer CC, Binkley N, McCloskey EV, Brandi M-L, Cooper C, et al. Trabecular bone score (TBS) as a new complementary approach for osteoporosis evaluation in clinical practice. Bone. 2015; 78: 216–224. https://doi.org/10.1016/j.bone.2015.05.016 PMID: 25988660
11. Hans D, Goertzen AL, Krieg M-A, Leslie WD. Bone microarchitecture assessed by TBS predicts osteoporotic fractures independent of bone density: the Manitoba study. Journal of Bone and Mineral Research. Wiley Online Library; 2011; 26: 2762–2769. https://doi.org/10.1002/jbmr.499 PMID: 21887701
12. Leslie WD, Aubry-Rozier B, Lix LM, Morin SN, Majumdar SR, Hans D. Spine bone texture assessed by trabecular bone score (TBS) predicts osteoporotic fractures in men: The Manitoba Bone Density Program. Bone. 2014; 67: 10–14. https://doi.org/10.1016/j.bone.2014.06.034 PMID: 24998455
13. Muschitz C, Kocijan R, Haschka J, Pahr D, Kaider A, Pietschmann P, et al. TBS reflects trabecular microarchitecture in premenopausal women and men with idiopathic osteoporosis and low-traumatic fractures. Bone. Elsevier; 2015; 79: 259–266. https://doi.org/10.1016/j.bone.2015.06.007 PMID: 26092650
14. Silva BC, Leslie WD, Resch H, Lamy O, Lesnyak O, Binkley N, et al. Trabecular bone score: a noninvasive analytical method based upon the DXA image. Journal of Bone and Mineral Research. Wiley Online Library; 2014; 29: 518–530. https://doi.org/10.1002/jbmr.2176 PMID: 24443324

15. Piodi LP, Poloni A, Ulivieri FM. Managing osteoporosis in ulcerative colitis: something new? World Journal of Gastroenterology: WJG. Baishideng Publishing Group Inc; 2014; 20: 14087. https://doi.org/10.3748/wjg.v20.i39.14087 PMID: 25339798

16. Graeff C, Marin F, Petto H, Kayser O, Reisinger A, Peña J, et al. High resolution quantitative computed tomography-based assessment of trabecular microstructure and strength estimates by finite-element analysis of the spine, but not DXA, reflects vertebral fracture status in men with glucocorticoid-induced osteoporosis. Bone. Elsevier; 2013; 52: 568–577. https://doi.org/10.1016/j.bone.2012.10.036 PMID: 23149277

17. Hosseini HS, Maquer G, Zysset PK. μCT-based trabecular anisotropy can be reproducibly computed from HR-pQCT scans using the triangulated bone surface. Bone. Elsevier; 2017; 97: 114–120. https://doi.org/10.1016/j.bone.2017.01.016 PMID: 28109918

18. Nishiyama KK, Shane E. Clinical imaging of bone microarchitecture with HR-pQCT. Current osteoporosis reports. Springer; 2013; 11: 147–155. https://doi.org/10.1007/s11914-013-0142-7 PMID: 23504496

19. Cohen A, Dempster D, Müller R, Guo X, Nickolas T, Liu X, et al. Assessment of trabecular and cortical architecture and mechanical competence of bone by high-resolution peripheral computed tomography: comparison with transiliac bone biopsy. Osteoporosis international. Springer; 2010; 21: 263–273. https://doi.org/10.1007/s00198-009-0945-7 PMID: 19455271

20. Müller R, Hildebrand T, Rüegsegger P. Non-Invasive bone biopsy: A new Method to Analyse and Display the Three-Dimensional structure of Trabecular Bone. Physics in Medicine and Biology. 1994; 39: 145–164. PMID: 7651993

21. Fields AJ, Eswaran SK, Jekir MG, Keaveny TM. Role of Trabecular Microarchitecture in Whole-Vertebral Body Biomechanical Behavior. Journal of Bone and Mineral Research. Wiley Online Library; 2009; 24: 1523–1530. https://doi.org/10.1359/jbmr.090317 PMID: 19338454

22. Keaveny TM, Morgan EF, Niebur GL, Yeh OC. Biomechanics of Trabecular Bone. Annual Review of Biomedical Engineering. 2001; 3: 307–333. https://doi.org/10.1146/annurev.bioeng.3.1.307 PMID: 11447066

23. Majumdar S, Genant H, Grampp S, Newitt D, Truong V-H, Lin J, et al. Correlation of trabecular bone structure with age, bone mineral density, and osteoporotic status: in vivo studies in the distal radius using high resolution magnetic resonance imaging. Journal of Bone and Mineral Research. Wiley Online Library; 1997; 12: 111–118. https://doi.org/10.1359/jbmr.1997.12.1.111 PMID: 9240733

24. Drews S, Matsuura M, Putz R. The trabecular architecture of the superior articular process of the lumbar spine (L2-S1). Surgical and Radiologic Anatomy. 2008; 30: 209–213. https://doi.org/10.1007/s00276-008-0317-6 PMID: 18299788

25. Harrigan TP, Mann RW. Characterisation of Microstructural Anisotropy in Orthotropic Materials Using a Second Rank Tensor. Journal of Materials Sciences. 1984; 19: 761–767.

26. Legrand E, Chappard D, Pascaretti C, Duquenne M, Krebs S, Rohmer V, et al. Trabecular Bone Microarchitecture, Bone Mineral Density and Vertebral Fractures in Male Osteoporosis. Journal of Bone and Mineral Research. 2000; 15: 13–19. https://doi.org/10.1359/jbmr.2000.15.1.13 PMID: 10646109

27. Whitehouse WJ. The quantitative morphology of anisotropic trabecular bone. Journal of Microscopy. Wiley Online Library; 1974; 101: 153–168. PMID: 4610138

28. Gdyczynski CM, Hashemi S, Manbachi A, Lashkari B, Cobbold RSC. On estimating the directionality distribution in pedicle trabecular bone from micro-CT images. Physiological Measurement. 2014; 35: 2415–2428. https://doi.org/10.1088/0967-3334/35/12/2415 PMID: 25391037

29. Hans D, Barthe N, Boutroy S, Pothuaud L, Winzenrieth R, Krieg M-A. Correlations between trabecular bone score, measured using anteroposterior dual-energy X-ray absorptiometry acquisition, and 3-dimensional parameters of bone microarchitecture: an experimental study on human cadaver vertebrae. Journal of Clinical Densitometry. Elsevier; 2011; 14: 302–312. https://doi.org/10.1016/j.jocd.2011.05.005 PMID: 21724435

30. Roux J, Wegrzyn J, Boutroy S, Bouxsein M, Hans D, Chapurlat R. The predictive value of trabecular bone score (TBS) on whole lumbar vertebrae mechanics: an ex vivo study. Osteoporosis International. Springer; 2013; 24: 2455–2460. https://doi.org/10.1007/s00198-013-2316-7 PMID: 23468074

31. Winzenrieth R, Michelet F, Hans D. Three-Dimensional (3D) Microarchitecture Correlations with 2D Projection Image Gray-Level Variations Assessed by Trabecular Bone Score Using High-Resolution Computed Tomographic Acquisitions: Effects of Resolution and Noise. Journal of Clinical Densitometry. 2013; 16: 287–296. https://doi.org/10.1016/j.jocd.2012.05.001 PMID: 22749406

32. Pothuaud L, Barthe N, Krieg M-A, Mehsen N, Carceller P, Hans D. Evaluation of the potential use of trabecular bone score to complement bone mineral density in the diagnosis of osteoporosis: a preliminary spine bmd–matched, case-control study. Journal of Clinical Densitometry. Elsevier; 2009; 12: 170–176. https://doi.org/10.1016/j.jocd.2008.11.006 PMID: 19181553

33. Silva BC, Broy SB, Boutroy S, Schousboe JT, Shepherd JA, Leslie WD. Fracture risk prediction by non-BMD DXA measures: the 2015 ISCD official positions part 2: trabecular bone score. Journal of Clinical Densitometry. Elsevier; 2015; 18: 309–330. https://doi.org/10.1016/j.jocd.2015.06.008 PMID: 26277849

34. Ulivieri FM, Silva BC, Sardanelli F, Hans D, Bilezikian JP, Caudarella R. Utility of the trabecular bone score (TBS) in secondary osteoporosis. Endocrine. Springer; 2014; 47: 435–448. https://doi.org/10.1007/s12020-014-0280-4 PMID: 24853880

35. Binkley N, Leslie WD. Clinical Application of Spine Trabecular Bone Score (TBS). Clinical Reviews in Bone and Mineral Metabolism. 2016; 14: 14–25. https://doi.org/10.1007/s12018-016-9203-7

36. Perilli E, Baleani M, Öhman C, Fognani R, Baruffaldi F, Viceconti M. Dependence of mechanical compressive strength on local variations in microarchitecture in cancellous bone of proximal human femur. Journal of Biomechanics. 2008; 41: 438–446. https://doi.org/10.1016/j.jbiomech.2007.08.003 PMID: 17949726

37. Teo JC, Si-Hoe KM, Keh JE, Teoh SH. Relationship between CT intensity, micro-architecture and mechanical properties of porcine vertebral cancellous bone. Clinical biomechanics. Elsevier; 2006; 21: 235–244. https://doi.org/10.1016/j.clinbiomech.2005.11.001 PMID: 16356612

38. Arlot ME, Burt-Pichat B, Roux J-P, Vashishth D, Bouxsein ML, Delmas PD. Microarchitecture influences microdamage accumulation in human vertebral trabecular bone. Journal of Bone and Mineral Research. Wiley Online Library; 2008; 23: 1613–1618. https://doi.org/10.1359/jbmr.080517 PMID: 18518771

39. Garrison JG, Gargac JA, Niebur GL. Shear strength and toughness of trabecular bone are more sensitive to density than damage. Journal of biomechanics. Elsevier; 2011; 44: 2747–2754. https://doi.org/10.1016/j.jbiomech.2011.09.002 PMID: 21945570

40. Karim L, Vashishth D. Role of trabecular microarchitecture in the formation, accumulation, and morphology of microdamage in human cancellous bone. Journal of Orthopaedic Research. Wiley Online Library; 2011; 29: 1739–1744. https://doi.org/10.1002/jor.21448 PMID: 21538510

41. Keaveny TM, Wachtel EF, Kopperdahl DL. Mechanical behavior of human trabecular bone after overloading. Journal of Orthopaedic Research. 1999; 17: 346–353. https://doi.org/10.1002/jor.1100170308 PMID: 10376722

42. Keaveny TM, Wachtel EF, Zadesky SP, Arramon YP. Application of the Tsai-Wu Quadratic Multiaxial Failure Criterion to Bovine Trabecular Bone. Journal of Biomechanical Engineering. 1999; 121: 99–107. PMID: 10080095

43. Burr DB, Turner CH, Naick P, Forwood MR, Ambrosius W, Hasan MS, et al. Does microdamage accumulation affect the mechanical properties of bone? Journal of Biomechanics. 1998; 31: 337–345. PMID: 9672087

44. Lee TC, O'Brien FJ, Gunnlaugsson T, Parkesh R, Taylor D. Microdamage and bone mechanobiology. Technology and Health Care. 2006; 14: 359–365. PMID: 17065757

45. Zioupos P, D CJ. The extent of microcracking and the morphology of microcracks in damaged bone. Journal of Material Siences. 1994; 29: 978–986.

46. Frost HM. A brief review for orthopedic surgeons: fatigue damage (microdamage) in bone (its determinants and clinical implications). Journal of Orthopaedic Science. 1998; 3: 272–281. PMID: 9732562

47. Kopperdahl DL, Pearlman JL, Keaveny TM. Biomechanical consequences of an isolated overload on the human vertebral body. Journal of Orthopaedic Research. 2000; 18: 685–690. https://doi.org/10.1002/jor.1100180502 PMID: 11117287

48. Keaveny TM, Wachtel EF, Guo XE, Hayes WC. Mechanical behavior of damaged trabecular bone. Journal of Biomechanics. 1994; 27: 1309–1318. PMID: 7798281

49. Moore TL, Gibson LJ. Modeling modulus reduction in bovine trabecular bone damaged in compression. Journal of Biomechanical Engineering. 2001; 123: 613–622. PMID: 11783733

50. Zysset PK. A constitutive law for trabecular bone. École Polytechnique Fédérale de Lausanne. 1994.

51. O'Brien FJ, Taylor D, Lee TC. The effect of bone microstructure on the initiation and growth of microcracks. Journal of Orthopaedic Research. 2005; 23: 475–480. https://doi.org/10.1016/j.orthres.2004.08.005 PMID: 15734265

52. Fyhrie DP, Schaffler MB. Failure mechanisms in human vertebral cancellous bone. Bone. 1994; 15: 105–109. PMID: 8024844

53. Nagaraja S, Couse TL, Guldberg RE. Trabecular bone microdamage and microstructural stresses under uniaxial compression. Journal of biomechanics. Elsevier; 2005; 38: 707–716. https://doi.org/10.1016/j.jbiomech.2004.05.013 PMID: 15713291

54. Zysset PK, Curnier A. A 3D damage model for trabecular bone based on fabric tensors. Journal of Biomechanics. 1996; 29: 1549–1558. PMID: 8945653

55. Mirzaali MJ, Bürki A, Schwiedrzik J, Zysset PK, Wolfram U. Contiuum Damage Interactions between Tension and Compression in Osteonal Bone. Journal of the Mechanical Behavior of Biomedical Materials. 2015; 49: 355–369. https://doi.org/10.1016/j.jmbbm.2015.05.007 PMID: 26093346

56. Wang X, Niebur GL. Microdamage Propagation in Trabecular Bone due to Changes in loading mode. Journal of Biomechanics. 2006; 39: 781–790. https://doi.org/10.1016/j.jbiomech.2005.02.007 PMID: 16488217

57. Wolfram U, Wilke H-J, Zysset PK. Damage accumulation in vertebral trabecular bone depends on loading mode and direction. Journal of Biomechanics. 2011; 44: 1164–1169. https://doi.org/10.1016/j.jbiomech.2011.01.018 PMID: 21295781

58. Busscher I, Ploegmakers JJ, Verkerke GJ, Veldhuizen AG. Comparative anatomical dimensions of the complete human and porcine spine. European Spine Journal. Springer; 2010; 19: 1104–1114. https://doi.org/10.1007/s00586-010-1326-9 PMID: 20186441

59. Looker A, Borrud L, Hughes J, Fan B, Shepherd J, Sherman M. Total body bone area, bone mineral content, and bone mineral density for individuals aged 8 years and over: United States, 1999–2006. Vital and health statistics Series 11, Data from the national health survey. 2013; 1–78. PMID: 25204772

60. Keaveny TM, Pinilla TP, Crawford RP, Kopperdahl DL, Lou A. Systematic and random errors in compression testing of trabecular bone. Journal of Orthopaedic Research. 1997; 15: 101–110. https://doi.org/10.1002/jor.1100150115 PMID: 9066533

61. Mirzaali MJ, Mussi V, Vena P, Libonati F, Vergani L, Strano M. Mimicking the loading adaptation of bone microstructure with aluminum foams. Materials & Design. Elsevier; 2017; 126: 207–218.

62. Abramoff MD, Magelhaes PJ, Ram SJ. Image Processing with ImageJ. Biophotonics International. 2004; 11: 36–42.

63. Doube M, Klosowski MM, Arganda-Carreras I, P CF, Dougherty RP, Jackson JS, et al. BoneJ: Free and extensible bone image analysis in ImageJ. Bone. 2010; 47: 1076–1079. https://doi.org/10.1016/j.bone.2010.08.023 PMID: 20817052

64. Otsu N. A threshold selection method from gray-level histograms. IEEE Transactions on Systems, Man, and Cybernetics. 1979; 9: 62–66.

65. Hildebrand T, Rüegesegger P. A new method for the model-independent assessment of thickness in three-dimensional images. Journal of Microscopy. 1997; 185: 67–75.

66. Lorensen WE, Cline HE. Marching Cubes: A High-Resolution 3D Surface Construction Algorithm. SIGGRAPH Comput Graph. ACM; 1987; 21: 163–169. https://doi.org/10.1145/37402.37422

67. Cowin SC. The relationship between the elasticity tensor and the fabric tensor. Mechanics of Materials. 1985; 4: 137–147.

68. Souzanchi MF, Palacio-Mancheno P, Borisov YA, Cardoso L, Cowin SC. Microarchitecture and Bone Quality in the Human Calcaneus: Local Variations of Fabric Anisotropy. Journal of bone and mineral research. 2012; 27: 2562–2572. https://doi.org/10.1002/jbmr.1710 PMID: 22807141

69. Badilatti SD, Christen P, Parkinson I, Müller R. Load-adaptive bone remodeling simulations reveal osteoporotic microstructural and mechanical changes in whole human vertebrae. Journal of biomechanics. Elsevier; 2016; 49: 3770–3779. https://doi.org/10.1016/j.jbiomech.2016.10.002 PMID: 27793404

70. Fyhrie D, Fazzalari N, Goulet R, Goldstein SA. Direct calculation of the surface-to-volume ratio for human cancellous bone. Journal of biomechanics. Elsevier; 1993; 26: 955–967. PMID: 8349720

71. Ryan G, Pandit A, Apatsidis D. Stress distribution in the intervertebral disc correlates with strength distribution in subdiscal trabecular bone in the porcine lumbar spine. Clinical Biomechanics. 2008; 23: 859–869. https://doi.org/10.1016/j.clinbiomech.2008.03.066 PMID: 18423954

72. Teo JCM, Si-Hoe KM, Keh JEL, Teoh SH. Relationship between {CT} intensity, micro-architecture and mechanical properties of porcine vertebral cancellous bone. Clinical Biomechanics. 2006; 21: 235–244. https://doi.org/10.1016/j.clinbiomech.2005.11.001 PMID: 16356612

73. Krueger D, Fidler E, Libber J, Aubry-Rozier B, Hans D, Binkley N. Spine trabecular bone score subsequent to bone mineral density improves fracture discrimination in women. Journal of Clinical Densitometry. Elsevier; 2014; 17: 60–65. https://doi.org/10.1016/j.jocd.2013.05.001 PMID: 23769698

74. Maquer G, Musy SN, Wandel J, Gross T, Zysset PK. Bone volume fraction and fabric anisotropy are better determinants of trabecular bone stiffness than other morphological variables. Journal of bone and mineral research. Wiley Online Library; 2015; 30: 1000–1008. https://doi.org/10.1002/jbmr.2437 PMID: 25529534

75. Nazarian A, Stauber M, Zurakowski D, Snyder BD, Müller R. The interaction of microstructure and volume fraction in predicting failure in cancellous bone. Bone. Elsevier; 2006; 39: 1196–1202. https://doi.org/10.1016/j.bone.2006.06.013 PMID: 16920051

76. Thurner PJ, Erickson B, Jungmann R, Schriock Z, Weaver JC, Fantner GE, et al. High-speed photography of compressed human trabecular bone correlates whitening to microscopic damage. Engineering fracture mechanics. Elsevier; 2007; 74: 1928–1941.

77. Wang X, Masse DB, Leng H, Hess KP, Ross RD, Roeder RK, et al. Detection of trabecular bone microdamage by micro-computed tomography. Journal of biomechanics. Elsevier; 2007; 40: 3397–3403. https://doi.org/10.1016/j.jbiomech.2007.05.009 PMID: 17588588

78. Wang X, Niebur GL. Microdamage propagation in trabecular bone due to changes in loading mode. Journal of biomechanics. Elsevier; 2006; 39: 781–790. https://doi.org/10.1016/j.jbiomech.2005.02.007 PMID: 16488217

79. Kinney J, Haupt D, Balooch M, Ladd A, Ryaby J, Lane N. Three-Dimensional Morphometry of the L6 Vertebra in the Ovariectomized Rat Model of Osteoporosis: Biomechanical Implications. Journal of Bone and Mineral Research. Wiley Online Library; 2000; 15: 1981–1991. https://doi.org/10.1359/jbmr.2000.15.10.1981 PMID: 11028451

80. Larrue A, Rattner A, Laroche N, Vico L, Peyrin F. Feasibility of micro-crack detection in human trabecular bone images from 3D synchrotron microtomography. Engineering in Medicine and Biology Society, 2007 EMBS 2007 29th Annual International Conference of the IEEE. IEEE; 2007. pp. 3918–3921.

81. Thurner PJ, Wyss P, Voide R, Stauber M, Stampanoni M, Sennhauser U, et al. Time-lapsed investigation of three-dimensional failure and damage accumulation in trabecular bone using synchrotron light. Bone. Elsevier; 2006; 39: 289–299. https://doi.org/10.1016/j.bone.2006.01.147 PMID: 16540385

82. Wolfram U, Schwiedrzik JJ, Mirzaali M, Bürki A, Varga P, Olivier C, et al. Characterizing microcrack orientation distribution functions in osteonal bone samples. Journal of microscopy. 2016; 264: 268–281. https://doi.org/10.1111/jmi.12440 PMID: 27421084

83. Fang G, Ji B, Liu XS, Guo XE. Quantification of trabecular bone microdamage using the virtual internal bond model and the individual trabeculae segmentation technique. Computer methods in biomechanics and biomedical engineering. Taylor & Francis; 2010; 13: 605–615. https://doi.org/10.1080/10255840903405660 PMID: 20077238

84. Hambli R. Micro-CT finite element model and experimental validation of trabecular bone damage and fracture. Bone. Elsevier; 2013; 56: 363–374. https://doi.org/10.1016/j.bone.2013.06.028 PMID: 23850483

85. Morgan EF, Yeh OC, Keaveny TM. Damage in trabecular bone at small strains. Jouropean Journal of Morphology. 2005; 42: 13–21.

86. Oftadeh R, Perez-Viloria M, Villa-Camacho JC, Vaziri A, Nazarian A. Biomechanics and mechanobiology of trabecular bone: a review. Journal of biomechanical engineering. American Society of Mechanical Engineers; 2015; 137: 010802.

87. Burr DB, Stafford T. Validity of the bulk-staining technique to separate artifactual from in vivo bone microdamage. Clinical Orthopaedics and Related Research. 1990; 305–308.

88. Goff M, Lambers F, Sorna R, Keaveny T, Hernandez C. Finite element models predict the location of microdamage in cancellous bone following uniaxial loading. Journal of biomechanics. Elsevier; 2015; 48: 4142–4148. https://doi.org/10.1016/j.jbiomech.2015.10.023 PMID: 26522622